Molecular Plant Advance Access published April 17, 2012

Structural and Functional Studies of the Mitochondrial Cysteine Desulfurase from *Arabidopsis thaliana*

Valeria R. Turowski, Maria V. Busi and **Diego F. Gomez-Casati**[1]

Centro de Estudios Fotosintéticos y Bioquímicos (CEFOBI–CONICET), Universidad Nacional de Rosario, Suipacha 531, 2000, Rosario, Argentina and Universidad Nacional de General San Martín (UNSAM), Av. Gral Paz 5445, San Martín, Buenos Aires, Argentina

ABSTRACT AtNfs1 is the *Arabidopsis thaliana* mitochondrial homolog of the bacterial cysteine desulfurases NifS and IscS, having an essential role in cellular Fe–S cluster assembly. Homology modeling of AtNfs1m predicts a high global similarity with *E. coli* IscS showing a full conservation of residues involved in the catalytic site, whereas the chloroplastic AtNfs2 is more similar to the *Synechocystis* sp. SufS. Pull-down assays showed that the recombinant mature form, AtNfs1m, specifically binds to *Arabidopsis* frataxin (AtFH). A hysteretic behavior, with a lag phase of several minutes, was observed and hysteretic parameters were affected by pre-incubation with AtFH. Moreover, AtFH modulates AtNfs1m kinetics, increasing V_{max} and decreasing the $S_{0.5}$ value for cysteine. Results suggest that AtFH plays an important role in the early steps of Fe–S cluster formation by regulating AtNfs1 activity in plant mitochondria.

Key words: cysteine desulfurase; Fe–S biogenesis; mitochondria; *Arabidopsis*; frataxin.

INTRODUCTION

Fe–S clusters are inorganic cofactors found in all kingdoms of life. These groups are part of a wide variety of proteins that participate in electron transfer, iron–sulfur storage, regulation of gene expression, photosynthesis, and enzyme activity (Johnson et al., 2005; Lill and Muhlenhoff, 2008; Ishimaru et al., 2009). The biosynthesis of Fe–S clusters requires a complex machinery and a growing number of genes involved in their synthesis have been identified (Balk and Lobreaux, 2005; Balk and Pilon, 2011). Three different types of Fe–S cluster biosynthetic systems have been described: (1) the NIF (nitrogen fixation) system, present in azothropic bacteria and required for metalocluster biogenesis in nitrogenase (Dos Santos et al., 2004; Rubio and Ludden, 2005); (2) the SUF (sulfur mobilization) system, originally identified in *E. coli* and also found in plastids; and (3) the ISC (iron–sulfur cluster) system, commonly found in bacteria and mitochondria from eukaryotic cells (Zheng et al., 1998; Patzer and Hantke, 1999; Takahashi and Tokumoto, 2002).

There are several steps that appear to be common to the three biosynthetic systems: the release of sulfur from cysteine, catalyzed by a cysteine desulfurase (NifS, Isc, SufS), and the transfer of sulfur to the scaffold proteins (named NifU, IscU, SUfA, NFU) where the iron–sulfur clusters are assembled (Balk and Lobreaux, 2005; Johnson et al., 2005; Balk and Pilon, 2011). In the last step, the mature Fe–S cluster is transferred and inserted into the apoprotein.

The NifS protein from *A. vinelandii* was shown to possess cysteine desulfurase activity that produces L-alanine and sulfur from L-cysteine. Thus, it was postulated that the physiological function of cysteine desulfurases is the supply of elemental sulfur to the Fe–S clusters (Zheng et al., 1993). In contrast to the wide description of different bacterial NifS and NifS-like proteins, there are only few studies on eukaryotic cysteine desulfurases, especially in photosynthetic organisms (Leon et al., 2002; Pilon-Smits et al., 2002; Muhlenhoff et al., 2004). The best-characterized NifS gene in eukaryotes is the mitochondrial *NFS1* from *S. cerevisiae*. It has been described that NFS1 is required for Fe–S protein activity but also for iron metabolism regulation (Li et al., 1999; Muhlenhoff et al., 2004).

Two genes coding for proteins with high similarity to NifS have been identified in Arabidopsis: AtNfs1 (At5g65720), located in mitochondria, and AtNfs2 (At1g08490), located in plastids (Kushnir et al., 2001; Leon et al., 2002). Leon et al. (2002) reported that AtNFS2 displays pyridoxal 5′ phosphate-dependent cysteine

[1] To whom correspondence should be addressed. E-mail gomezcasati@cefobi-conicet.gov.ar, tel. +54 341 437-1955, fax +54 341 437-0044.

doi: 10.1093/mp/sss037
Received 10 August 2011; accepted 2 March 2012

desulfurase activity and is able to act as a sulfur donor for Fe–S biogenesis *in vitro* (Abdel-Ghany et al., 2005). Moreover, it has been described that AtNFs2 interacts with the CpSufE protein, and that this interaction increases the catalytic efficiency of AtNFs2 (Ye et al., 2006). Thus, it has been suggested that the AtNfs2–CpSufE complex forms a cysteine desulfurase required for Fe–S cluster formation in chloroplasts. Xu and Moller (2006) demonstrated that CpSufE localizes in plastids and mitochondria in tobacco leaves and its overexpression in *Arabidopsis* affects AtNfs1 and AtNfs2 levels. Indeed, it has been described that CpSufE activates both cysteine desulfurases *in vitro* and is required for chloroplast Fe–S cluster protein maturation (Xu and Moller, 2006; Ye et al., 2006).

Previous studies have shown that the frataxin gene is required for the *de novo* biogenesis of cellular Fe–S proteins *in vivo* (Muhlenhoff et al., 2002). Moreover, we recently characterized the *Arabidopsis* frataxin homolog and its essential role for full activity of mitochondrial Fe–S proteins (Busi et al., 2004, 2006; Maliandi et al., 2007). It has been reported that the yeast frataxin homolog (Yfh1) specifically binds to the central Fe–S cluster assembly complex, which is composed of the scaffold protein Isu1 and the cysteine desulfurase Nfs1, and that this interaction is increased in the presence of ferrous iron (Gerber et al., 2003). There is a controversy about the exact function of frataxin. Recently, Tsai and Barondeau reported that human frataxin activates the Fe–S cluster formation and that frataxin levels regulate the ISC complex activity and stimulates cysteine desulfurase in the presence of Fe^{2+}. It is worth noting that oxidizing conditions diminish the level of ISC complex formation and frataxin activation (Tsai and Barondeau, 2010). However, it has also been proposed that frataxin is an iron sensor that negatively regulates Fe–S cluster formation without affecting the cysteine desulfurase activity (Adinolfi et al., 2009; Prischi et al., 2010). In the present study, we characterized the structure and function of the mature form of AtNfs1 (AtNfs1m). We detected a high topological conservation of the 3-D AtNfs1 model when compared with the *E. coli* cysteine desulfurase (IscS) 3-D structure, showing a fully conserved structure of the active site region, whereas AtNfs2 shows a different structure, with high similarity to *Synechocystis* SufS. In addition, we report that AtNfs1 interacts with *Arabidopsis* frataxin homolog (AtFH) and that this interaction modulates AtNfs1 kinetic properties. These data suggest a direct role of AtFH in the regulation of the mitochondrial cysteine desulfurase, which could be relevant to Fe–S formation in plants.

RESULTS

Sequence Analysis and Homology Modeling of AtNfs1 and AtNfs2

A homology model of the AtNfs1 protein was built as described in the 'Methods' section using the 3-D structure of IscS, a cysteine desulfurase from *E. coli* (PDB code 1P3W, 50% identity for residues 15–335) (Cupp-Vickery et al., 2003). Analysis using the Verify 3D program showed 100% of positive score values, 93% of these higher than 0.2 (overall score 0.42), while a Z-score of –10.49 was obtained using Prosa II. According to these results, we found that the AtNfs1 model is of good quality. The monomeric AtNfs1 model exhibited a fold similar to IscS with both α-helical and β-sheet secondary structures conserved (Figure 1A). An alignment of the polypeptide backbone structures of AtNfs1 and IscS showed that both 3-D structures are very similar (Figure 1B). This alignment was performed using the main chain atoms of residues 52–441 for AtNfs1 and 2–392 for IscS. The catalytic Cys377 residue, equivalent to Cys328 of IscS, is well conserved. However, the region containing the Cys residue (amino acids 328–333) was omitted in the original model developed for IscS (and also in the AtNfs1 model), since it is disordered and did not display sufficient electron density for model building. It has been postulated that this disorder may reflect a requirement for high flexibility in order to function in catalysis and desulfuration, as well as in the transfer of bound persulfide to acceptor proteins (Cupp-Vickery et al., 2003). A closer view of the superposed active site region of both the AtNfs1 model and the template IscS is shown in Figure 1C. All amino acid residues postulated to be part of the active site pocket (Thr124, His152, Lys153, Asn203, Glu204, Gln231, Lys254, and Tyr386, AtNfs1 numbering) are well conserved.

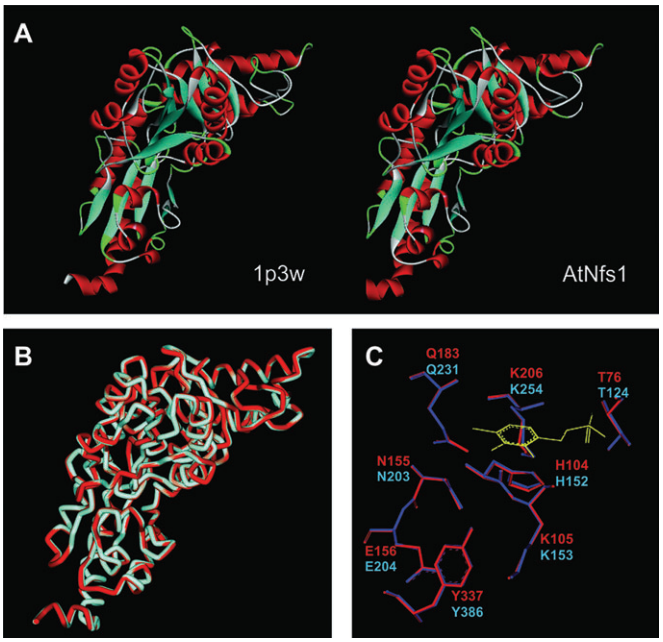

Figure 1. Homology Modelling of AtNfs1.

(A) Structural model of *E. coli* IscS (PDB 1P3W, left) and the proposed model for AtNfs1 (right).

(B) Superposition of IscS (red) and AtNfs1 (cyan) structures.

(C) Superposition between AtNfs1 model and IscS structure showing the residues involved in the active site. AtNfs1 residues are shown in blue and IscS residues are shown in red. Representation of bound PLP is shown in yellow.

In order to compare the 3-D structure of AtNfs1 with the chloroplastic cysteine desulfurase, we also constructed a homology model of AtNfs2. The amino acid sequence alignment of AtNfs2 showed that it has only 19% of identity when compared to IscS (Figure 2). Thus, the attempts to get a valid 3-D structure of AtNfs2 using IscS as protein template did not result in a valid model. Therefore, we have built a homology model of AtNfs2 using the 3-D structure of the *Synechocystis* sp. PCC 6803 SufS enzyme (PDB code 1T3I, 63% identity for residues 8–414) (Tirupati et al., 2004). Analysis using the Verify 3D program showed 99% of positive score values, being 94% of these higher than 0.2 (overall score 0.45). In addition, a Z-score of –8.84 was obtained using Prosa II, indicating the good quality of the model. Figure 3A shows that the monomeric AtNfs2 model exhibited a fold similar to SufS, also displaying a high structural similarity when the backbone structures were superimposed (Figure 3B). Moreover, the amino acids postulated to be involved in the active site are also well conserved, with the exception of the Thr181 residue (Val225 in AtNfs2) (Figure 3C). It is interesting to note that, when considering the mitochondrial and the chloroplastic cysteine desulfurases, both active sites have similar structures showing a high conservation of many residues involved in the catalytic site: Gln231, Lys-254, Thr-124, Asn203, and His152 (from AtNfs1) are well conserved in AtNFs2, whereas the Lys153 and Glu204 (from AtNfs1) are replaced by His173 and V225, respectively, in AtNfs2 (see Figures 1C and 3C).

Cloning and Expression of Mature AtNfs1 (AtNfs1m)

The DNA fragment containing the AtNfs1m sequence was cloned in a pDEST17 vector containing an N-terminal His_6-tag to generate plasmid pVRT01. AtNfs1m contains 419 amino acid residues but lacks the N-terminal transit peptide for mitochondrial localization. Predictive analysis of the AtNfs1 amino acidic sequence using the MITOPROT program identified a putative transit peptide of 34 amino acids (score

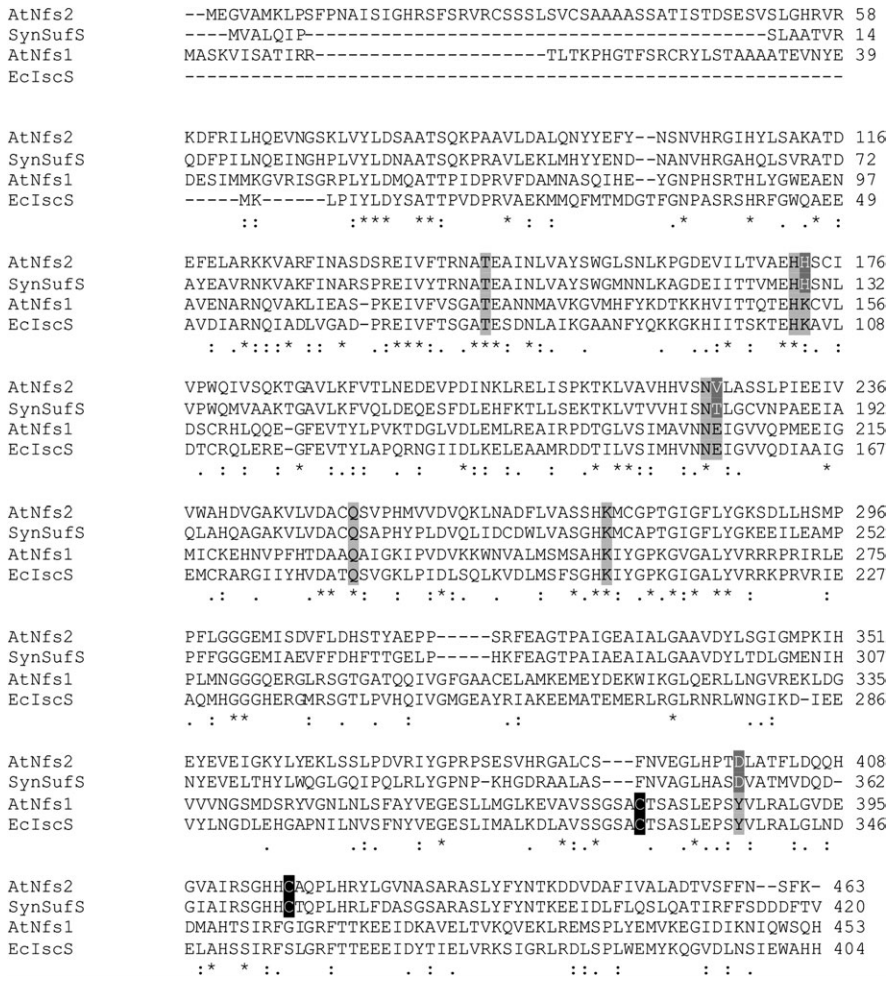

Figure 2. Amino Acidic Sequence Alignment of Cysteine Desulfurases from Groups I and II.

The amino acidic sequences of AtNFS1 (At5g65720) and *E. coli* IscS (P0A6B7) from group I were compared with AtNfs2 (At1g08490) and SynSufS (Q55793) from group II. Conserved residues into the active site region (see Figures 1C and 2C) are shaded in light gray and those partially conserved are boxed in dark gray with white letters. Cysteines involved in catalysis are indicated in black boxes and white letters. Alignment was performed using the ClustalW2 program (www.ebi.ac.uk/Tools/msa/clustalw2/).

0.9914) (Claros and Vincens, 1996). Attempts to purify AtNfs1m from the soluble phase resulted in the degradation of the protein to lower molecular mass peptides as shown in Supplemental Figure 1. Therefore, in order to avoid degradation of AtNfs1m, we carried out the expression and purification of this protein as detailed in the 'Methods' section. The pVRT01 plasmid was expressed in *E. coli* BL21(DE3) RIL cells and the protein was purified using a HiTrap chelating column. It is important to note that native soluble AtNfs1m did not bind to the resin, but shows a positive binding under denatured conditions. This procedure yielded about 1.2 mg of purified AtNfs1m per gram of cells. Figure 4 (lanes 1–7) shows an SDS–PAGE analysis of the soluble and insoluble fractions from *E. coli* cells expressing AtNfs1m. Lane 8 shows the presence of AtNfs1m after its solubilization from inclusion bodies. Lane 9 shows a single protein band with the expected molecular mass (47 kDa) purified from inclusion bodies. The presence of recombinant AtNfs1m was confirmed by immunoblotting (Lane 10).

In order to evaluate the correct folding of the recombinant AtNfs1m protein, we analyzed its secondary structure by circular dichroism (CD). Figure 5 shows the CD spectrum for the protein renatured in the presence of the pyridoxal 5′phosphate (PLP) cofactor (Figure 5, continuous line), while the spectrum of the renatured protein in the absence of PLP was similar to that obtained for the partially denatured enzyme. It is important to note that we could not measure any enzymatic activity when AtNfs1m was refolded in the absence of PLP. These findings indicate that the cofactor is required for the correct folding of AtNfs1m.

To analyze the data from the CD spectrum of the refolded protein, we estimated the percentages of the secondary structure using the K2d algorithm (Andrade et al., 1993). The content of alpha helices, beta sheets, and random coil were 44, 16, and 40%, respectively, being similar to those predicted from the AtNfs1 model (42% alpha helix, 12% beta sheets, and 46% random coil). Taking into account that the average error between the values obtained from the CD spectrum and the model was lower than that obtained for the secondary structure prediction using K2d ($0.036 < 0.122$), these results show that the secondary structure of the refolded recombinant protein is consistent with the predicted structure obtained by homology modeling.

Interaction Between AtNfs1m and AtFH

It has been reported that Yfh1 specifically binds to the central Fe/S cluster (ISC)-assembly complex composed by Isu1/Nfs1 (Gerber et al., 2003). To investigate the existence of a possible protein-protein interaction between AtNfs1 and AtFH, an in vitro pull down assay using purified AtFH-His6 (Maliandi et al., 2007) and an extract expressing recombinant AtNfs1 lacking the histidine tag was used. We determined a positive interaction between AtNfs1m and AtFH (Figure 6A), and this result was also confirmed by Western blotting (Figure 6B). After incubation of the AtNfs1m extract with the Ni^{2+} resin containing AtFH, two protein bands were observed by SDS–PAGE analysis (Figure 6A, lane 1): a 47-kDa band corresponding to AtNfs1m and a 14-kDa band corresponding to AtFH. Incubation of an *E. coli* cell extract lacking AtNfs1m with AtFH and the Ni^{2+} resin is shown in lane 2. The absence of protein bands other than AtFH indicates that the interaction is specific

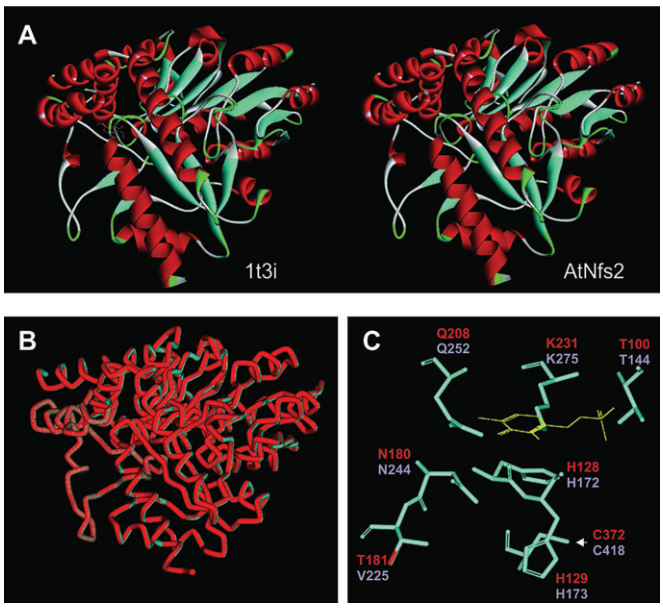

Figure 3. Homology Modelling of AtNfs2.

(A) Structural model of *Synechocystis* sp. SufS (PDB 1T3I, left) and proposed model for AtNfs2 (right).

(B) Superposition of SufS (red) and AtNfs2 (cyan) structures.

(C) Superposition between AtNfs2 model and SufS structure showing residues involved in the active site. AtNfs2 residues are shown in cyan and SufS residues in red. PLP is shown in yellow. The arrow indicates the position of Cys372 (SufS) and Cys418 (AtNfs2) involved in catalysis.

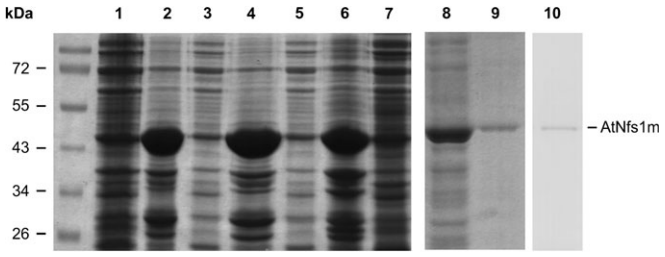

Figure 4. Expression Analysis of Recombinant AtNfs1m from *E. coli* Cells.

The different *E. coli* cell extracts were electrophoresed on SDS–PAGE and revealed with Coomassie blue staining. Lane 1: Bacterial proteins without induction; Lanes 2, 4, and 6: insoluble proteins after 3, 6, and 16-h induction. Lanes 3, 5, and 7: soluble proteins after 3, 6, and 16-h induction. Lane 8: Proteins obtained after the solubilization of inclusion bodies. Lane 9: SDS–PAGE of recombinant purified AtNfs1m; Lane 10: Western blot analysis of AtNfs1m followed by incubation with anti-penta-His antibodies. Numerals on the left indicate molecular masses of the standards (PageRuler Prestained Protein Ladder, Fermentas).

and eliminates the possibility of non-specific interactions with *E. coli* IscS. Incubation of the AtNfs1m extract with the Ni^{2+} resin alone did not show the presence of any protein band (lane 3).

Effect of AtFH on AtNfs1m Kinetic Parameters

Figure 7A shows a time course of the reaction catalyzed by AtNfs1m. As shown, a hysteretic behavior with a lag phase of several minutes was observed in these experiments. Absorbance variations displayed non-linear reaction rates when assays were initiated by the addition of AtNfs1m. Under these conditions, the enzyme reached maximal activity values after a lag period, which was shortened or eliminated by increasing AtFH concentrations. Thus, the addition to the pre-incubation medium of a 1:1 or 1:3 AtNfs1m:AtFH molar ratio modified AtNfs1m kinetic behavior. Enzyme kinetics followed a first-order exponential increase (Figure 7A, inset), since the data follow the equation described by Neet and Ainslie (1980): $\ln(Vss - V) = \ln(Vss - Vi) - t/\tau$, where V, Vi, and Vss are the instantaneous, initial, and steady-state (linear) velocities, respectively; t symbolizes time of the reaction and τ represents the inverse of the apparent rate constant for the transition between Vi and Vss (Gomez-Casati et al., 2000). Table 1 shows Vi, Vss, and τ values calculated using the described equation for the time course of AtNfs1m activity in the absence or presence of AtFH. Incubation of AtNfs1m with AtFH (1:3) decreased the τ value almost 15-fold and also increased Vss nearly twofold (Table 1). Figure 7B displays the fold change

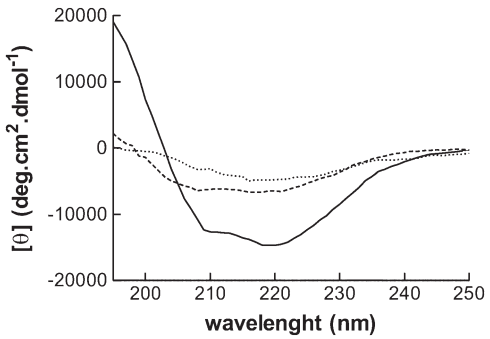

Figure 5. Far-UV CD Spectra of Recombinant AtNfs1m.

Protein samples were dialyzed in the absence (dashed line) or presence (solid line) of 0.5 mM pirydoxal 5′ phosphate. An aliquot of enzyme refolded with cofactor was partially denatured by boiling for 5 min (dotted line) and included as control.

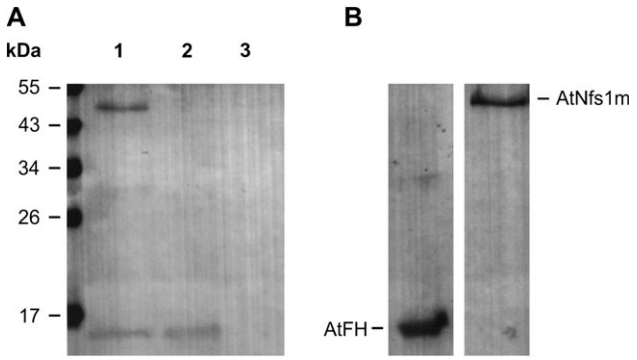

Figure 6. Investigation of Protein-protein Interaction Between AtNfs1 and AtFH.

(A) SDS–PAGE analysis of pull-down assays of recombinant AtFH and AtNfs1m proteins. The AtNfs1m protein was recovered together with AtFH (lane 1). Lane 2 shows the recovered AtFH bound to the Ni^{2+} resin after incubation with an *E. coli* cell extract lacking AtNfs1m. Lane 3 shows the absence of nonspecifically bound proteins (control).

(B) Western blot analysis illustrating the presence of AtFH and AtNfs1m, using anti-FH and anti-AtNfs1m, respectively.

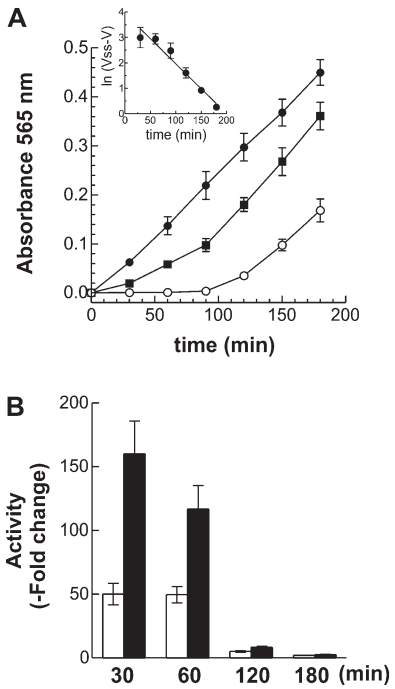

Figure 7. Hysteretic Behavior of AtNfs1m

(A) Time course of the reaction catalyzed by AtNfs1m pre-incubated without AtFH (white circles) or with a 1:1 (black squares) or 1:3 (black circles) AtNfs1m:AtFH molar ratio. Production of L-alanine was followed spectrophotometrically as described in the 'Methods' section. Inset: fitting of the time course plot of AtNfs1m incubated in the absence of AtFH to the equation developed by Neet and Ainslie (1980) for enzymes exhibiting hysteretic behavior.

(B) Fold change in AtNfs1m activity derived from Figure 6A, in the presence of 1:1 (white bars) or 1:3 (black bars) molar amounts of AtFH in the pre-incubation medium.

Table 1. Effect of AtFH on the Hysteretic Properties Exhibited by AtNfs1m.

Effector	τ (min)	Vi (mU mg^{-1})	Vss (mU mg^{-1})
n.a.	255.9 ± 18.5	0.11 ± 0.02	20.5 ± 1.9
AtFH (1:1)[a]	133.6 ± 11.2	7.5 ± 0.9	33.9 ± 2.8
AtFH (1:3)[a]	17.5 ± 1.3	33.3 ± 4.3	36.7 ± 3.2

a molar ratio AtNfs1m:AtFH; n.a., no addition.

in AtNfs1m activity (*V*) in the presence of 1:1 or 1:3 molar amounts of AtFH in the pre-incubation medium. Results show that, at 30 or 60 min, the presence of AtNfs1m:AtFH (1:1) increases the activity of the enzyme almost 50-fold compared with AtNfs1m alone, whereas the protein mixture containing AtNfs1m:AtFH (1:3) showed a 160- and 117-fold increase in enzymatic activity at 30 or 60 min, respectively. Finally, a five- or twofold increase in AtNfs1m catalytic activity was observed at 120 or 180 min, respectively.

When AtNfs1m kinetic parameters were determined in the presence of variable concentrations of cysteine, the enzyme displayed a $S_{0.5}$ value of 0.73 ± 0.08 mM; n_H of 1.7 ± 0.3 and V_{max} of 21.2 ± 1.7 mU mg^{-1}. Saturation plots were performed using the V_{ss} obtained from the time course plots at different cysteine concentrations (Figure 8). When AtFH was added to the assay medium, AtNfs1m displayed Michaelis-Menten kinetics and a twofold decrease in the $S_{0.5}$ value for cysteine was determined. In addition, we found a nearly twofold increase in V_{max}. Thus, there is an almost threefold increase in the catalytic efficiency of AtNfs1m in the presence of AtFH (Figure 8 and Table 2).

DISCUSSION

Several studies have reported the presence of NifS proteins catalyzing the formation of L-alanine and sulfur from L-cysteine (Mihara et al., 1997; Nakai et al., 1998; Leon et al., 2002; Mihara and Esaki, 2002; Pilon-Smits et al., 2002). In addition, cysteine has been described as the substrate for Fe–S cluster formation within cells and cysteine desulfurase as the enzyme performing this step (Zheng et al., 1993; Johnson et al., 2005; Lill and Muhlenhoff, 2008). The NifS family proteins are classified into two groups, I and II, on the basis of sequence similarity and the amino acid analysis of a protein motif in the active site that contains a conserved Cys (Mihara et al., 1997). The *Arabidopsis* genome codifies for two cysteine desulfurases, namely AtNfs1 and AtNfs2. AtNfs1, the mitochondrial cysteine desulfurase, shows 50% identity compared to IscS from *E. coli* (included in group I of the cysteine desulfurases) (Cupp-Vickery et al., 2003). In contrast, AtNfs2 shows low identity (19%) compared to IscS, whereas a high sequence identity (63%) compared with SufS from *Synechocystis* was observed, indicating that AtNfs2 is structurally and sequentially different from AtNfs1. This is in agreement with the classification of AtNfs2 within group II of the cysteine desulfurases (Leon et al., 2002; Mihara and Esaki, 2002; Pilon-Smits et al., 2002). Here, we found that the structural model obtained for AtNfs1 possesses a high global similarity to *E. coli* IscS, showing a full conservation of the residues comprising the active site. This suggests the existence of similar substrate and PLP binding interactions in AtNfs1 and IscS.

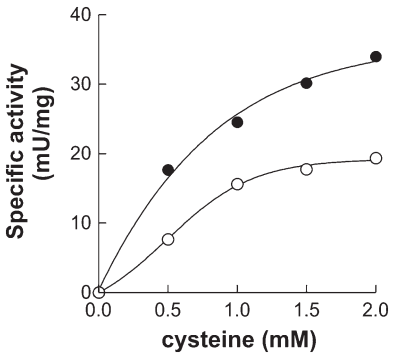

Figure 8. L-alanine Production from L-Cysteine Catalyzed by AtNfs1m, Performed in the Absence (White Circles) or Presence (Black Circles) of AtFH (1:3 AtNfs1m:AtFH Molar Ratio).

One unit of activity is defined as the amount of enzyme catalyzing the production of 1 μmol of L-alanine per minute at 37°C.

Table 2. Kinetic Parameters of AtNfs1m Using Cysteine as Substrate, in the Presence or Absence of AtFH.

Effector	$S_{0.5}$ (mM)	n_H	V_{max} (mU mg^{-1})	$V_{max}/S_{0.5}$
n.a.	0.73 ± 0.08	1.7 ± 0.3	21.2 ± 1.7	29.0 ± 5.5
+ AtFH*	0.44 ± 0.03	1.0 ± 0.2	37.1 ± 2.9	84.3 ± 12.3

* A 1:3 molar amount of AtNfs1m:AtFH was used in the assay medium; n.a., no addition.

Amino acid sequence alignment along with comparison of the structures of the four proteins mentioned above indicates that the residues involved in the active site are well conserved, although there are some striking features, such as the replacement of Lys105/153 and Glu156/204 in EcIscS/AtNfs1 by His129/173 and by Thr181/Val225 in SynSufS/AtNfs2. The change in Lys105/153 by His129/173 could have structural importance because this residue is located very closely to the cysteine involved in catalysis. Vickery et al. (Cupp-Vickery et al., 2003) reported that the change of Lys105 (from IscS) to an His124 in the CsdB, another group II cysteine desulfurase from *E. coli*, might contribute to a decreased mobility of the catalytic cysteine, possibly reflecting different catalytic mechanisms (Fujii et al., 2000; Cupp-Vickery et al., 2003). Moreover, the structural differences found in the catalytic region of AtNfs1 and AtNfs2 reflect a different evolutionary origin, which agrees with the endosymbiotic theory of the origin of mitochondria and chloroplasts proposed by Margulis (1970) several decades ago. The postulate is in accordance with the location of AtNfs1 and AtNfs2 on different branches of the phylogenetic tree as shown in the work by Leon et al. (2002) and Pilon-Smits et al. (2002).

The CD studies showed that recombinant AtNfs1m has a similar proportion of the different secondary structures to those described for *E. coli* IscS obtained by X-ray crystallography (40.1% alpha helices and 13.8% beta sheets) (Cupp-Vickery et al., 2003). In addition, AtNfs1m requires PLP for its correct folding, similarly to other PLP transferase-like proteins (Greenfield and Fasman, 1969) (see also http://scop.berkeley.edu/sunid=53383). Taken together, these results indicate that AtNfs1 could be part of the family of PLP-dependent transferase-like α/β proteins as well as their homologs IscS from *E. coli* and NifS from *T. maritima* (Kaiser et al., 2000; Cupp-Vickery et al., 2003).

Recently, two recombinant AtNfs1 proteins have been cloned and their specific activities determined (1) a full-length AtNfs1 and (2) a thioredoxin fusion protein (TRX–AtNfs1). Full-length AtNfs1 contains the predicted 34 amino acid mitochondrial transit peptide (Xu and Moller, 2006) with no detectable AtNfs1 activity in cysteine desulfurization assays and a specific activity of 3 nmol min^{-1} mg^{-1} $protein^{-1}$ in the presence of AtSufE (CpSufE) (Xu and Moller, 2006). On the other hand, the thioredoxin fusion protein (TRX–AtNfs1) shows a specific activity of 12 nmol min^{-1} mg^{-1} $protein^{-1}$ in the absence of regulators (Frazzon et al., 2007). In our work, we report that AtNfs1m has a specific activity of 21.2 nmol min^{-1} mg^{-1} protein, which is increased by AtFH. Moreover, AtFH decreases the $S_{0.5}$ value for cysteine and the value obtained (0.44 mM) is between four- and 10-fold higher compared with that reported for the chloroplastic isoform AtNfs2 in the absence or presence of the activator AtSufE (Ye et al., 2006). There are no available data about the apparent affinity of AtNfs1 for cysteine. The almost undetectable AtNfs1 activity observed by Xu and Moller (2006) could be due to the short incubation period used to measure sulfide release (30 min). It is worth noting that enzyme activity is undetectable in under 120 min. Our results are in agreement with those reported by Frazzon et al. (2007), where TRX–AtNfs1 activity was measured 150 min after the addition of L-cysteine. The existence of a more active form of the enzyme could be due to either the lack of fused TRX or the predicted 34 amino acid transit peptide in the AtNfs1m recombinant protein. In addition, AtNfs1m interaction with and activation by AtFH point to a functional AtNfs1m:AtFH complex. This is in agreement with evidence indicating that YFH binds to the Isu1/Nfs1 complex in *S. cerevisiae* (Gerber et al., 2003). In support of this, we found an induction of *AtNfs1* mRNA expression in AtFH-deficient plants, indicating the existence of a genetic link between both genes. Moreover, the interaction of yeast Nfs1 with a small protein of unknown function (Isd11) was reported using pull-down techniques (Wiedemann et al., 2006). It has been reported that Isd11 has an essential role in Fe–S cluster biogenesis in mitochondria, since its absence caused a strong reduction in several Fe–S proteins and also the decrease in the enzymatic activities of aconitase and SDH. In addition, the formation of Fe–S clusters on ISU1 is decreased in *isd11-1*-deficient yeasts, indicating that Isd11 is required at an early stage of biogenesis of Fe–S groups (Wiedemann et al., 2006). Recently, Richards et al. reported a bioinformatic analysis of Isd11, demonstrating the presence of this protein in different eukaryotic organisms, including plants and algae. Moreover, the presence in eukaryotes of Isd11 as a functional partner to IscS directly implies a single shared α-proteobacterial endosymbiotic ancestry for all eukaryotes (Richards and van der Giezen, 2006).

It has been suggested that frataxin and cysteine desulfurase could be involved in early steps of Fe–S cluster formation, more specifically iron loading and sulfur transfer to the scaffold proteins, probably ISU homologs, and subsequent transfer to apoproteins (Gerber et al., 2003). Previous research indicates that the *Arabidopsis* genome contains ISU1, ISU2, and ISU3 genes, all three localized in mitochondria and with high sequence similarity to IscU/Isu (Balk and Lobreaux, 2005; Leon et al., 2005; Frazzon et al., 2007). Thus, in accordance with the existence of a conserved Fe–S biogenesis process in plant mitochondria, it is likely that the same ISU-dependent mechanism occurs in this organelle.

Kinetic analysis of purified AtNfs1m showed a hysteretic behavior with a lag phase of several minutes. Hysteresis is known to have physiological significance in damping radical changes in metabolite concentration in biological systems (Neet and Ainslie, 1980). It has been described that other NifS homologs exhibit non-Michaelis kinetics and hysteretic behavior (Mihara et al., 2000). The transient lag showed by AtNfs1m was dependent on AtFH concentration in the pre-incubation medium. Thus, it is possible to postulate that AtNfs1 exists in two conformations: a low-activity form, in the absence of AtFH, and a high-activity form, triggered by AtFH binding. The significance of the hysteretic behavior of AtNfs1 under *in vivo* conditions is not clear. However, the interaction between AtFH and AtNfs1m could represent a unique regulatory mechanism in which the lack of AtFH binding prevents the premature activation of AtNfs1 and its presence would be involved in a complex mechanism activating this cysteine desulfurase. This might be a special adaptation to the specific metabolic requirements of plant mitochondria for the biogenesis of Fe–S clusters.

METHODS

Plant Material and Bacterial Strains

A. thaliana (var. Columbia Col-0), grown in a greenhouse, was used in these experiments. *Escherichia coli* BL21-(DE3)-RIL strain (*E. coli* B F– *ompT hsdS*(rB– mB) *dcm*+ Tetr *gal* (DE3) *endA* Hte (*argU ileY leuW* Camr)) was used in this study.

Cloning, Expression, and Purification of Mature AtNfs1 (AtNfs1m)

Total RNA extracted from *Arabidopsis* leaves was used as template for cDNA synthesis using random hexamers. The cDNA (1257 bp) was PCR amplified using Pfu polymerase (Promega) and the following primers: nfsfw: 5′-GGGGACAAGTTTGTACAAAAAAGCAGGCTCAGAGGTGAATTACGAGGATG-3′ and nfsrv: 5′-GGGGACCACTTTGTACAAGAAAGCTGGGTATCAGTGTTGAGACCATTGAA-3′. The resulting PCR product was cloned into pDonr221 by recombination using the Gateway BP clonase reaction according to the manufacturer's instructions (Gateway Technology, Invitrogen). The AtNfs1 insert into the Gateway entry clone was transferred by recombination into the pDEST17 vector using the LR clonase reaction. The new vector named pVRT01 encodes AtNfs1m (Arabidopsis thaliana mitochondrial cysteine desulfurase, mature form, amino acids 35–453, containing an N-terminal His-tag sequence) without the predicted transit peptide.

Purification of AtNfs1 and AtFH

E. coli BL21(DE3) RIL cells harboring plasmid pVRT01 were grown at 37°C in LB medium containing 100 μg ml^{-1} ampicillin and 35 μg ml^{-1} chloramphenicol to an OD_{600} = 0.6. AtNFS1m production was induced by the addition of 1 mM IPTG and subsequent incubation for 18 h at 30°C. Cells were harvested and re-suspended in 20 mM Tris-HCl, pH 7.4, containing 1 mM phenylmethylsulfonyl fluoride (PMSF), disrupted by sonication and centrifuged at 7000 *g* for 15 min at 4°C. The pellet obtained was re-suspended in 10 ml of 20 mM Tris-HCl, pH 7.4, 8 M urea and incubated with gentle shaking for 2 h at 25°C and then centrifuged at 10 000 *g* for 30 min at 4°C. In order to perform AtNfs1m purification, the clarified *E. coli* extract was centrifuged again (10 000 *g* for 30 min at 4°C) and loaded onto a HiTrap chelating column (GE Healthcare). The column was washed with 20 ml of 20 mM Tris-HCl, pH 7.4, 8 M urea, 20 mM imidazole and the recombinant protein was eluted by an imidazole gradient (20–500 mM) in 20 mM Tris-HCl, pH 7.4, containing 8 M urea. Purified fractions were collected and sequentially dialyzed at 4°C against decreasing concentrations of urea (8–0 M) in 20 mM Tris-HCl, pH 7.4, 0.5 mM PLP, 0.5 M NaCl, 20% glycerol. The presence of the enzyme was monitored in chromatography fractions by activity and SDS–PAGE analysis. The purified enzyme was pooled and concentrated to >1 mg ml^{-1}, stored at –20°C, and its activity remained stable for at least 1 month. AtFH protein was produced and purified as described previously (Maliandi et al., 2007).

Cysteine Desulfurase Assay

AtNfs1m activity was assayed using a medium containing 25 mM Tris-HCl, pH 8, 100 mM NaCl, 10 μM PLP, 100 μM DTT, and different amounts of recombinant AtFH (0–50 μg) and cysteine (0–2 mM) when indicated. Assays were initiated by the addition of enzyme and were incubated at 37°C for different times (0–180 min). Different enzyme concentrations were tested to ensure steady-state conditions. L-alanine production from L-cysteine was quantified by a modified colorimetric ninhydrin method (Moore and Stein, 1948; Sheng et al., 1993). Briefly, one reaction volume of ninhydrine in ethanol (0.2% W/V) was added to supernatants, incubated at 100°C for 30 min, centrifuged, and maintained on ice until measuring OD_{565}. According to the data reported by Moore and Stein (1948), the cysteine–ninhydrin mixtures showed no significant OD at 565 nm. L-alanine concentration was estimated from a standard curve from 0 to 2 mM obtained under the same conditions as described above. One unit of activity is defined as the amount of enzyme catalyzing the production of 1 μmol of L-alanine per minute at 37°C. The kinetic parameters, $S_{0.5}$, n_H, and V_{max} were calculated as described (Brooks, 1992). The specific activity (V_{max}) of the enzyme was calculated using the steady-state (linear) velocities, V_{ss} at 2 mM cysteine. To plot AtNfs1 activity versus substrate concentration, the V_{ss} obtained for each cysteine concentration was used. All determinations were performed at least in triplicate and average values ± SD are reported.

Pull-Down Assays

Pull-down assays were carried out as described previously (Wayllace et al., 2010). Briefly, purified His_6-tagged AtFH was bound to a Ni^{2+}-Sepharose high-performance resin (GE Healthcare Bio-Sciences) previously equilibrated with binding buffer (20 mM NaH_2PO_4, pH 7.4, 50 mM NaCl, 1 mM 2-mercaptoethanol, and 20 mM imidazole), followed by incubation with about 1 mg of a protein extract from *E. coli* BL21 (DE3) RIL cells transformed with AtNfs1m in pET32 lacking the His_6-tag. After washing three times with binding buffer, the resin was centrifuged for 3 min at 500 *g* and the supernatant discarded. Bound proteins were eluted from the resin by the addition of 300 mM imidazole, and subjected to SDS–PAGE analysis and immunoblotting.

Circular Dichroism (CD)

Far-UV CD spectra were obtained using a Jasco J-810 spectropolarimeter (Jasco International Co.) over the wavelength range from 195 to 250 nm, at 25°C. Measurements were performed in a 0.2-cm quartz cuvette at a rate of 100 nm min^{-1}, bandwidth of 1 nm, response time of 2 s, data pitch of 1 nm, and accumulation of 10. CD data are shown as the mean residue ellipticity (deg cm^2 $dmol^{-1}$) obtained after subtracting the baseline, smoothing, and data normalization.

CD spectra for AtNfs1m (0.1–1 mg ml^{-1}) were recorded in 20 mM Na-phosphate buffer, pH 7.4. To obtain AtNfs1m partially denatured, the sample refolded in the presence of PLP was boiled for 5 min. Secondary structure analysis from CD spectra data was performed using the K2d algorithm (Andrade et al., 1993). Percentages of alpha helices, beta sheets, and random coils were compared with those predicted from the AtNfs1 model using the PSIPRED v 3.0 program (http://bioinf.cs.ucl.ac.uk/psipred).

Additional Methods

SDS–PAGE was performed using 12% gels as described by Laemmli (1970). Gels were developed by Coomassie blue staining or electro-blotted onto nitrocellulose membranes (Bio-Rad). Electro-blotted membranes were incubated with penta-His antibody (Qiagen) or polyclonal anti-AtFH antibodies (Maliandi et al., 2007). The antigen–antibody complex was visualized with alkaline phosphatase-linked anti-mouse IgG or anti-rabbit IgG, followed by staining with BCIP and NBT (Bollag et al., 1996). Total protein concentration was determined as described by Bradford (1976). Statistical analyses: significant differences were determined using Student's *t*-test. Values statistically different from the control ($P < 0.05$) are denoted with an asterisk. 3-D structural models were obtained using the Modeller program using T.I.T.O. (Tool for Incremental Threading Optimisation) for the alignment between query and template (Labesse and Mornon, 1998; Douguet and Labesse, 2001). Models were evaluated with the ProSA-web structure analysis program (Sippl, 1993; Wiederstein and Sippl, 2007) and Verify-3D (Luthy et al., 1992). Superposition of

AtNfs1/IscS and AtNfs2/SufS structures was performed using the SuperPose server v 1.0 (Maiti et al., 2004).

SUPPLEMENTARY DATA

Supplementary Data are available at *Molecular Plant Online.*

FUNDING

This work was supported by grants from ANPCyT (PICT 00614 and 0729).

ACKNOWLEDGMENTS

VRT is a Doctoral fellow from CONICET. M.V.B. and D.G.C. are research members from CONICET. No conflict of interest declared.

REFERENCES

Abdel-Ghany, S.E., Ye, H., Garifullina, G.F., Zhang, L., Pilon-Smits, E.A., and Pilon, M. (2005). Iron–sulfur cluster biogenesis in chloroplasts: involvement of the scaffold protein CpIscA. Plant Physiol. **138,** 161–172.

Adinolfi, S., et al. (2009). Bacterial frataxin CyaY is the gatekeeper of iron–sulfur cluster formation catalyzed by IscS. Nat. Struct. Mol. Biol. **16,** 390–396.

Andrade, M.A., Chacon, P., Merelo, J.J., and Moran, F. (1993). Evaluation of secondary structure of proteins from UV circular dichroism spectra using an unsupervised learning neural network. Protein Eng. **6,** 383–390.

Balk, J., and Lobreaux, S. (2005). Biogenesis of iron–sulfur proteins in plants. Trends Plant Sci. **10,** 324–331.

Balk, J., and Pilon, M. (2011). Ancient and essential: the assembly of iron–sulfur clusters in plants. Trends Plant Sci. **16,** 218–226.

Bollag, D.M., Rozycki, M.D., and Edelstein, S.J. (1996). Protein Methods (New York: Wiley-Liss).

Bradford, M.M. (1976). A rapid and sensitive method for the quantitation of microgram quantities of protein utilizing the principle of protein-dye binding. Anal. Biochem. **72,** 248–254.

Brooks, S.P. (1992). A simple computer program with statistical tests for the analysis of enzyme kinetics. Biotechniques. **13,** 906–911.

Busi, M.V., et al. (2006). Deficiency of *Arabidopsis thaliana* frataxin alters activity of mitochondrial Fe–S proteins and induces oxidative stress. Plant J. **48,** 873–882.

Busi, M.V., Zabaleta, E.J., Araya, A., and Gomez-Casati, D.F. (2004). Functional and molecular characterization of the frataxin homolog from *Arabidopsis thaliana*. FEBS Lett. **576,** 141–144.

Claros, M.G., and Vincens, P. (1996). Computational method to predict mitochondrially imported proteins and their targeting sequences. Eur. J. Biochem. **241,** 779–786.

Cupp-Vickery, J.R., Urbina, H., and Vickery, L.E. (2003). Crystal structure of IscS, a cysteine desulfurase from *Escherichia coli*. J. Mol. Biol. **330,** 1049–1059.

Dos Santos, P.C., Dean, D.R., Hu, Y., and Ribbe, M.W. (2004). Formation and insertion of the nitrogenase iron-molybdenum cofactor. Chem. Rev. **104,** 1159–1173.

Douguet, D., and Labesse, G. (2001). Easier threading through web-based comparisons and cross-validations. Bioinformatics. **17,** 752–753.

Frazzon, A.P., et al. (2007). Functional analysis of *Arabidopsis* genes involved in mitochondrial iron–sulfur cluster assembly. Plant Mol. Biol. **64,** 225–240.

Fujii, T., Maeda, M., Mihara, H., Kurihara, T., Esaki, N., and Hata, Y. (2000). Structure of a NifS homologue: X-ray structure analysis of CsdB, an *Escherichia coli* counterpart of mammalian selenocysteine lyase. Biochemistry. **39,** 1263–1273.

Gerber, J., Muhlenhoff, U., and Lill, R. (2003). An interaction between frataxin and Isu1/Nfs1 that is crucial for Fe/S cluster synthesis on Isu1. EMBO Rep. **4,** 906–911.

Gomez-Casati, D.F., Sesma, J.I., and Iglesias, A.A. (2000). Structural and kinetic characterization of NADP-dependent, non-phosphorylating glyceraldehyde-3-phosphate dehydrogenase from celery leaves. Plant Sci. **154,** 107–115.

Greenfield, N., and Fasman, G.D. (1969). Computed circular dichroism spectra for the evaluation of protein conformation. Biochemistry. **8,** 4108–4116.

Ishimaru, Y., et al. (2009). Rice-specific mitochondrial iron-regulated gene (MIR) plays an important role in iron homeostasis. Mol. Plant. **2,** 1059–1066.

Johnson, D.C., Dean, D.R., Smith, A.D., and Johnson, M.K. (2005). Structure, function, and formation of biological iron–sulfur clusters. Annu. Rev. Biochem. **74,** 247–281.

Kaiser, J.T., Clausen, T., Bourenkow, G.P., Bartunik, H.D., Steinbacher, S., and Huber, R. (2000). Crystal structure of a NifS-like protein from *Thermotoga maritima*: implications for iron sulphur cluster assembly. J. Mol. Biol. **297,** 451–464.

Kushnir, S., et al. (2001). A mutation of the mitochondrial ABC transporter Sta1 leads to dwarfism and chlorosis in the *Arabidopsis* mutant starik. Plant Cell. **13,** 89–100.

Labesse, G., and Mornon, J. (1998). Incremental threading optimization (TITO) to help alignment and modelling of remote homologues. Bioinformatics. **14,** 206–211.

Laemmli, U.K. (1970). Cleavage of structural proteins during the assembly of the head of bacteriophage T4. Nature. **227,** 680–685.

Leon, S., Touraine, B., Briat, J.F., and Lobreaux, S. (2002). The AtNFS2 gene from *Arabidopsis thaliana* encodes a NifS-like plastidial cysteine desulphurase. Biochem. J. **366,** 557–564.

Leon, S., Touraine, B., Briat, J.F., and Lobreaux, S. (2005). Mitochondrial localization of *Arabidopsis thaliana* Isu Fe–S scaffold proteins. FEBS Lett. **579,** 1930–1934.

Li, J., Kogan, M., Knight, S.A., Pain, D., and Dancis, A. (1999). Yeast mitochondrial protein, Nfs1p, coordinately regulates iron–sulfur cluster proteins, cellular iron uptake, and iron distribution. J. Biol. Chem. **274,** 33025–33034.

Lill, R., and Muhlenhoff, U. (2008). Maturation of iron–sulfur proteins in eukaryotes: mechanisms, connected processes, and diseases. Annu. Rev. Biochem. **77,** 669–700.

Luthy, R., Bowie, J.U., and Eisenberg, D. (1992). Assessment of protein models with three-dimensional profiles. Nature. **356,** 83–85.

Maiti, R., Van Domselaar, G.H., Zhang, H., and Wishart, D.S. (2004). SuperPose: a simple server for sophisticated structural superposition. Nucleic Acids Res. **32,** W590–W594.

Maliandi, M.V., Busi, M.V., Clemente, M., Zabaleta, E.J., Araya, A., and Gomez-Casati, D.F. (2007). Expression and one-step purification of recombinant *Arabidopsis thaliana* frataxin homolog (AtFH). Protein Expr. Purif. **51,** 157–161.

Margulis, L. (1970). Origin of Eukaryotic Cells (New Haven, CT: Yale University Press).

Mihara, H., and Esaki, N. (2002). Bacterial cysteine desulfurases: their function and mechanisms. Appl. Microbiol. Biotechnol. **60,** 12–23.

Mihara, H., Kurihara, T., Yoshimura, T., and Esaki, N. (2000). Kinetic and mutational studies of three NifS homologs from *Escherichia coli*: mechanistic difference between L-cysteine desulfurase and L-selenocysteine lyase reactions. J. Biochem. **127,** 559–567.

Mihara, H., Kurihara, T., Yoshimura, T., Soda, K., and Esaki, N. (1997). Cysteine sulfinate desulfinase, a NIFS-like protein of *Escherichia coli* with selenocysteine lyase and cysteine desulfurase activities: gene cloning, purification, and characterization of a novel pyridoxal enzyme. J. Biol. Chem. **272,** 22417–22424.

Moore, S., and Stein, W.H. (1948). Photometric ninhydrin method for use in the chromatography of amino acids. J. Biol. Chem. **176,** 367–388.

Muhlenhoff, U., et al. (2004). Functional characterization of the eukaryotic cysteine desulfurase Nfs1p from *Saccharomyces cerevisiae*. J. Biol. Chem. **279,** 36906–36915.

Muhlenhoff, U., Richhardt, N., Ristow, M., Kispal, G., and Lill, R. (2002). The yeast frataxin homolog Yfh1p plays a specific role in the maturation of cellular Fe/S proteins. Hum. Mol. Genet. **11,** 2025–2036.

Nakai, Y., Yoshihara, Y., Hayashi, H., and Kagamiyama, H. (1998). cDNA cloning and characterization of mouse nifS-like protein, m-Nfs1: mitochondrial localization of eukaryotic NifS-like proteins. FEBS Lett. **433,** 143–148.

Neet, K.E., and Ainslie, G.R., Jr (1980). Hysteretic enzymes. Methods Enzymol. **64,** 192–226.

Patzer, S.I., and Hantke, K. (1999). SufS is a NifS-like protein, and SufD is necessary for stability of the [2Fe-2S] FhuF protein in *Escherichia coli*. J. Bacteriol. **181,** 3307–3309.

Pilon-Smits, E.A., et al. (2002). Characterization of a NifS-like chloroplast protein from *Arabidopsis*: implications for its role in sulfur and selenium metabolism. Plant Physiol. **130,** 1309–1318.

Prischi, F., et al. (2010). Structural bases for the interaction of frataxin with the central components of iron–sulphur cluster assembly. Nat. Commun. **1,** 95.

Richards, T.A., and van der Giezen, M. (2006). Evolution of the Isd11-IscS complex reveals a single alpha-proteobacterial endosymbiosis for all eukaryotes. Mol. Biol. Evol. **23,** 1341–1344.

Rubio, L.M., and Ludden, P.W. (2005). Maturation of nitrogenase: a biochemical puzzle. J. Bacteriol. **187,** 405–414.

Sheng, S., Kraft, J.J., and Schuster, S.M. (1993). A specific quantitative colorimetric assay for L-asparagine. Anal. Biochem. **211,** 242–249.

Sippl, M.J. (1993). Recognition of errors in three-dimensional structures of proteins. Proteins. **17,** 355–362.

Takahashi, Y., and Tokumoto, U. (2002). A third bacterial system for the assembly of iron–sulfur clusters with homologs in archaea and plastids. J. Biol. Chem. **277,** 28380–28383.

Tirupati, B., Vey, J.L., Drennan, C.L., and Bollinger, J.M., Jr (2004). Kinetic and structural characterization of Slr0077/SufS, the essential cysteine desulfurase from *Synechocystis* sp. PCC 6803. Biochemistry. **43,** 12210–12219.

Tsai, C.L., and Barondeau, D.P. (2010). Human frataxin is an allosteric switch that activates the Fe–S cluster biosynthetic complex. Biochemistry. **49,** 9132–9139.

Wayllace, N.Z., Valdez, H.A., Ugalde, R.A., Busi, M.V., and Gomez-Casati, D.F. (2010). The starch-binding capacity of the noncatalytic SBD2 region and the interaction between the N- and C-terminal domains are involved in the modulation of the activity of starch synthase III from *Arabidopsis thaliana*. FEBS J. **277,** 428–440.

Wiedemann, N., et al. (2006). Essential role of Isd11 in mitochondrial iron–sulfur cluster synthesis on Isu scaffold proteins. EMBO J. **25,** 184–195.

Wiederstein, M., and Sippl, M.J. (2007). ProSA-web: interactive web service for the recognition of errors in three-dimensional structures of proteins. Nucleic Acids Res. **35,** W407–W410.

Xu, X.M., and Moller, S.G. (2006). AtSufE is an essential activator of plastidic and mitochondrial desulfurases in *Arabidopsis*. EMBO J. **25,** 900–909.

Ye, H., Abdel-Ghany, S.E., Anderson, T.D., Pilon-Smits, E.A., and Pilon, M. (2006). CpSufE activates the cysteine desulfurase CpNifS for chloroplastic Fe–S cluster formation. J. Biol. Chem. **281,** 8958–8969.

Zheng, L., Cash, V.L., Flint, D.H., and Dean, D.R. (1998). Assembly of iron–sulfur clusters: identification of an iscSUA–hscBA–fdx gene cluster from *Azotobacter vinelandii*. J. Biol. Chem. **273,** 13264–13272.

Zheng, L., White, R.H., Cash, V.L., Jack, R.F., and Dean, D.R. (1993). Cysteine desulfurase activity indicates a role for NifS in metallocluster biosynthesis. Proc. Natl Acad. Sci. U S A. **90,** 2754–2758.